International Journal of Fatigue 188 (2024) 108531

Contents lists available at ScienceDirect

International Journal of Fatigue

journal homepage: www.elsevier.com/locate/ijfatigue

# In vitro corrosion-fatigue behaviour of rare-earth containing magnesium WE43 in sterile complex cell culture medium

Julia Nachtsheim [a], Songyun Ma [a,*], Jaka Burja [b,c], Alexander Kopp [d,e], Jan-Marten Seitz [d], Bernd Markert [a]

[a] Institute of General Mechanics, RWTH Aachen University, Eilfschornsteinstraße 18, 52062 Aachen, Germany
[b] Institute of Metals and Technology, Lepi pot 11, 1000 Ljubljana, Slovenia
[c] Department of Materials and Metallurgy, Faculty of Natural Sciences and Engineering, University of Ljubljana, Aškerčeva cesta 12, 1000 Ljubljana, Slovenia
[d] Medical Magnesium GmbH, Philipsstraße 8, 52068 Aachen, Germany
[e] Meotec GmbH, Philipsstraße 8, 52068 Aachen, Germany

ARTICLE INFO

*Keywords:*
Corrosion-fatigue behaviour
Stress corrosion mechanisms
Biodegradable magnesium alloys
WE43
DMEM

ABSTRACT

Rare-earth containing magnesium alloys are promising biomedical materials for a new generation of biodegradable orthopaedic implant systems due to their excellent biocompatibility, mechanical and biodegradation properties. However, chemo-mechanical interactions in aggressive physiological corrosion environments result in rapid degradation and early loss of mechanical integrity, limiting its broader application for orthopaedic implants. To date, only few studies have assessed the corrosion-fatigue behaviour of medical-grade magnesium alloys in an organic physiological corrosion environment, especially under sterile test conditions. In the present work, the corrosion-fatigue behaviour of fine-grained medical-grade magnesium alloy WE43MEO was systematically analysed under in vitro conditions using an organic physiological fluid DMEM. The experimental results showed that the fatigue strength of the alloy is nearly unaffected by a 1-day precorrosion, while a 7-day precorrosion resulted in a significant deterioration of mechanical integrity. In corrosion-fatigue experiments, the fatigue life was considerably reduced by interactions between corrosion and fatigue damages. The SEM analysis revealed that the mixed mode of intergranular and transgranular fracture in the crack propagation zone transits to intergranular cracking dominant mode under the corrosion-fatigue conditions due to hydrogen embrittlement.

## 1. Introduction

Designing biodegradable orthopaedic implant systems of magnesium alloys is a current challenge in biomedical engineering. The highly biocompatible magnesium implants are resorbed by the human body during the service period, eliminating the necessity for implant removal surgery. Magnesium alloys significantly decrease pathological tissue development caused by stress-shielding, which is induced by mismatching mechanical properties between implant material and bone tissue. Additionally, bone formation and integration are improved [1–3]. In the biodegradation process of the implant, the alloy constituents will be metabolised by the human body. Hence, the amount of implanted alloying elements must be kept within physiologically tolerable levels [4]. The use of aluminium-containing alloys is controversial in biomedical applications, since aluminium has been identified as potentially neurotoxic and carcinogenic [5,6]. As a consequence, more aluminium-free magnesium alloys have been developed to meet the essential biocompatibility requirements. As rare-earth containing alloys are considered as one of the most promising materials, more systematic studies on magnesium alloys with rare-earth elements are required for facilitate the magnesium implant development [7–9].

Despite significant progress in the development of biodegradable magnesium alloys, a major challenge for broader application in orthopaedic implants is the fast degradation of mechanical integrity in aggressive physiological corrosion environments. The loss of mechanical integrity is dramatically accelerated by the synergetic effect arising from the superposition of mechanical stresses during corrosion [10]. The resulting chemo-mechanical interactions can lead to stress corrosion cracking (SCC) and corrosion-fatigue (CF) during implant service. Implant failure can occur at loads significantly below the material's strength in static or quasi-static loading conditions. Although the complex mechano-chemical degradation during cyclic loadings is of great

* Corresponding author.
*E-mail address:* ma@iam.rwth-aachen.de (S. Ma).

https://doi.org/10.1016/j.ijfatigue.2024.108531
Received 16 May 2024; Received in revised form 18 July 2024; Accepted 25 July 2024
Available online 26 July 2024

importance for the adequate design of orthopaedic implants, the CF behaviour of medical-grade magnesium alloys in physiological environments has not been thoroughly studied and understood so far, especially in an organic corrosion environment. First single-piece biodegradable magnesium implants for cardiovascular and orthopaedic applications were successfully approved by Conformité Européene (CE) [11]. To expand the CE-marked products for load-bearing implants and multi-part implant systems, the CF behaviour of medical-grade magnesium alloys needs to be studied more extensively.

Recent studies indicate that the interaction between corrosion and fatigue in a physiological environment can significantly accelerate the damage evolution of magnesium alloys [12]. Chen et al. [13] reported that the elongation-to-failure and the fatigue life of the magnesium alloy AZ31B in SBF were significantly reduced in comparison with the results in air. It was concluded that the detrimental effect is attributed to the interaction between corrosion and ratcheting strain as well as the rupture of the corrosion product layer in SBF with physiological pH values. Gu et al. [14] demonstrated that both magnesium alloys WE43 and AZ91D have a much lower fatigue strength in SBF and exhibit higher corrosion rates under dynamic loading conditions. Furthermore, the CF behaviour of magnesium alloys is strongly affected by microstructural features. Wang et al. [15] characterised the influence of microstructural changes after solution treatments on CF of an Mg-Zn-Y-Zr alloy. It is shown that coarse and homogeneous grains in the solution-treated alloy were prone to trigger twinning and localised corrosion at the twin boundaries, leading to an acceleration of CF failure. Moreover, the loading conditions play an important role in the CF interaction. In particular, low loading frequencies result in severe corrosion damage and a significant decrease in fatigue strength [16]. Linderov et al. [17] concluded that low frequencies should be used in CF tests to better understand the interactions of corrosion mechanism, stress corrosion mechanisms and CF mechanism.

In experimental studies on the corrosion performance of biodegradable magnesium alloys for medical applications, the impact of fluid constituents has been extensively investigated [18–27]. Meng et al. [28] analysed the influence of the solution pH on the CF performance of an AM60 alloy. It was shown that an instable protective layer in phosphate-buffered saline solution with acidic pH significantly increased the corrosion rate during CF experiments and reduced the fatigue life. Organic compounds, being important constituents of the human body, significantly affect the corrosion behaviour of magnesium alloys [29–32]. The addition of proteins and amino acids leads to the formation of hybrid inorganic–organic corrosion products, which provide superior corrosion protection compared to purely inorganic corrosion products [33]. Therefore, it is suggested that they be added to the fluids for in vitro SCC or CF studies. Chen et al. [34] identified the formation of a hybrid inorganic–organic corrosion product layer in in vitro corrosion experiments on magnesium alloys, which provides better protection against SCC compared to the purely inorganic corrosion layer in inorganic solutions. Harandi et al. [35] found that in CF experiments on magnesium alloys, the protein bovine serum albumin initially adsorbed to the protective layer, stabilising the protective layer and delaying the corrosion attack. These findings encourage the use of organic fluids in CF experiments for a better approximation of in vivo conditions. However, the high contamination risks and the commonly non-sterile experimental setups limit the application of organic fluids in SCC or CF experiments [34].

The magnesium alloy WE43MEO with an excellent combination of high strength and ductility was systematically assessed for its biocompatibility and biodegradability in in vitro and in vivo studies [36–39]. However, material degradation under cyclic loadings, which is crucial for a safe implant design, has not yet been investigated. More experimental studies on the complex mechano-chemical degradation of this alloy under cyclic loadings in physiological environments are needed to extend the category of biodegradable magnesium implants for load-bearing applications. More importantly, most in vitro experiments used the corrosion medium without relevant organic compounds in body fluids, which significantly affect the corrosion behaviour in in vivo conditions.

In this study, we systematically investigated the in vitro corrosion-fatigue behaviour of the medical-grade magnesium alloy WE43MEO in sterile DMEM. To the knowledge of the authors, this is the first study to investigate the corrosion-fatigue behaviour of the rare-earth containing magnesium alloy WE43 in a sterile complex cell culture medium with organic compounds. Furthermore, the effects of precorrosion with different immersion periods on the fatigue performance of the alloy were studied to understand the degradation process of mechanical integrity. The corrosion-fatigue behaviour and mechanisms in the corrosion fluid DMEM were analysed by using scanning electron microscopy. The experimental setup and procedure for corrosion-fatigue tests in aseptic conditions is presented in our work. The present study provides valuable information and data on the corrosion-fatigue behaviour of the medical-grade magnesium alloy WE43MEO for the biomechanical design of biodegradable implants.

## 2. Materials and methods

Round fatigue specimens with a diameter of 2.5 mm shown in Fig. 1 were designed according to DIN 50125 and fabricated by Medical Magnesium GmbH (Aachen, Germany) from 9.5 mm rods of a clinically used extruded magnesium alloy WE43MEO (Meotec GmbH, Aachen), which is alloyed with rare-earth elements. The alloy is manufactured considering the following elemental specifications: 1.4 – 4.2 wt% Y, 2.5 – 3.5 wt% Nd, $<$ 1 wt% for Al, Fe, Cu, Ni, Mn, Zn, Zr and Mg as balance. Stress and strain-controlled fatigue tests in air were conducted to study cyclic deformation and fatigue behaviour of the fine-grained magnesium alloy. In order to evaluate the effect of precorrosion damage on the fatigue behaviour of the alloy, a number of fatigue specimens were immersed in the corrosive environment for different periods before fatigue testing. In addition, the interaction between the corrosion and fatigue processes was investigated in CF experiments.

### 2.1. Fatigue tests in air

Stress-controlled fatigue tests in air were performed on an MTS Minibionix II testing machine (MTS Systems GmbH, Germany), controlled by FlexTest 60 (MTS Systems Corp., Minneapolis, USA). Corresponding sample elongation was measured with an optical extensometer (GOM Aramis SRX Adjustable, Carl Zeiss GOM Metrology GmbH, Germany). Fatigue tests were performed at room temperature with an axial tensile sinusoidal loading and a stress ratio of R=0. Tests were performed until failure or stopped after $2x10^6$ cycles. Strain-controlled fatigue tests in air were performed at room temperature on an INSTRON 8802 test machine equipped with 250 kN load cell. The stress amplitudes for the fatigue tests in air were selected to cover the fatigue data from the low cycle fatigue to high cycle fatigue regimes.

### 2.2. Precorrosion experiments

To study the effect of precorrosion on the fatigue behaviour, the fatigue specimens were immersed in 500 ml of pre-heated (37 °C) complex cell culture fluid Dulbecco's Modified Eagle's Medium (DMEM,

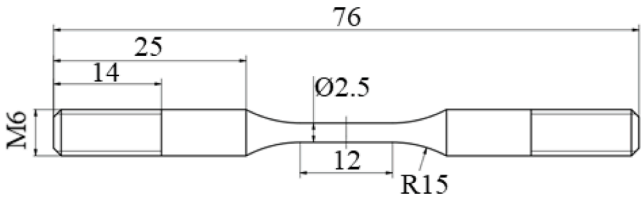


**Fig. 1.** Geometry of the fatigue specimen, dimensions given in mm.

L0101-500, Biowest, Nuaillé, France), which uses a bicarbonate buffer system. The fluid was supplemented with 5 ml Penicillin-Streptomycin (ThermoFisher Scientific Inc., Waltham, MA, USA) and 5 ml Amphotericin B (ThermoFisher Scientific Inc., Waltham, MA, USA). A comparison of the ionic concentrations of DMEM and human body plasma and the overall composition of the DMEM is given in [40]. The experimental setup is shown in Fig. 2a. To limit the exposed specimen surface to the central part, both specimen ends were sealed using Teflon tape. Experimental equipment was carefully sterilised before each experiment. The experiment was assembled under sterile working conditions in a clean bench class 100 equipped with HEPA-filter and then placed in an incubator with a steady temperature of 37 °C ± 1 °C. Gas exchange between the corrosion environment and the incubator atmosphere was allowed via a filtering cap. After precorrosion periods of either 1 or 7 days, specimens were removed from the fluid, washed with distilled water, then with 90 % ethanol and air-dried subsequently.

### 2.3. Corrosion-fatigue experiments

An inhouse developed setup was used for CF experiments, which ensures a sterile corrosion environment in the corrosion cell (shown in Fig. 2b). The setup and the sterile procedure are described in more detail in [41]. Fatigue specimens were installed on a test bench, equipped with a force transducer (Model 661.20F-03, MTS Systems Corp., Minneapolis, USA) and controlled by FlexTest 60 (MTS Systems Corp., Minneapolis, USA). CF tests were performed stress-controlled at a frequency of 1 Hz, which corresponds to the walking frequency of an adult. The stress amplitudes in the corrosion-fatigue tests for assessing the influence of the corrosive environment on the fatigue behaviour were selected to compare with the fatigue performance in air under similar stress levels. In the further work, the corrosion-fatigue tests with the stress amplitudes experienced under in vivo conditions should be conducted for the design of specific biodegradable orthopaedic implants. 650 ml DMEM, supplemented with 5 ml Penicillin-Streptomycin and 5 ml Amphotericin B, was used as corrosion fluid at a temperature of 37 °C ± 1 °C. The pH value was controlled optically using the phenol red colour indicator in the DMEM fluid, and the experiments with an unphysiological pH regime or contaminations were excluded from the analysis. After failure, specimens were removed from the fluid and washed with distilled water, then with 90 % ethanol and then air-dried.

### 2.4. Fractography

Fracture surfaces were analysed by scanning electron microscopy and back-scatter electron microscopy using a Zeiss CrossBeam 550 (Carl Zeiss AG, Oberkochen, Germany). Samples for transmission electron microscopy (TEM) were prepared using argon ion-slicing with JEOL EM 09100IS Ion Slicer and observed with TEM (JOEL JEM 2100).

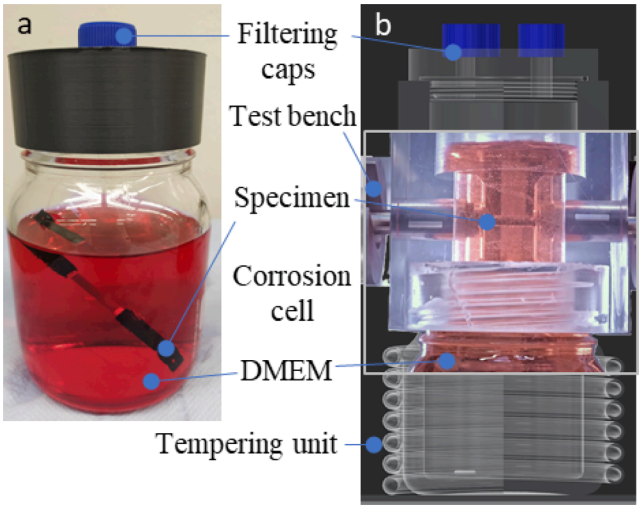


**Fig. 2.** (a) Experimental setup for precorrosion positioned in an incubator. (b) Experimental setup of corrosion-fatigue experiments.

## 3. Results and discussion

### 3.1. Microstructure

Fig. 3 shows the alpha-magnesium matrix with an average grain size of 2.7 µm and intermetallic Mg-Y-Nd precipitates of less than 0.1 µm in diameter. Precipitates are found at grain boundaries as well as inside grains. EDS analysis revealed that neodymium is predominantly present in the intermetallic participates of Mg–Y–Nd at concentrations of up to 27 wt% and the content of yttrium is similar in the alpha-matrix and in the precipitates [41].

### 3.2. Strain-controlled fatigue in air

Fig. 4a shows stabilised stress–strain hysteresis of strain-controlled fatigue tests at different strain amplitudes between 0.6 % and 1.4 %. The cyclic stress–strain curve is fitted by the Ramberg-Osgood equation using the material parameters of cyclic strengthening coefficient $K'$ and the cyclic hardening coefficient $n'$ [42]:

$$\varepsilon_a = \varepsilon_a^e + \varepsilon_a^p = \frac{\sigma}{E} + \left(\frac{\sigma}{K'}\right)^{1/n'} \quad (1)$$

with the strain amplitude $\varepsilon_a$, the elastic strain amplitude $\varepsilon_a^e$, the plastic strain amplitude $\varepsilon_a^p$, the axial stress σ and the elastic modulus $E$.

The comparison between cyclic and monotonic stress–strain curves indicates a cyclic softening behaviour of the material. The S-N curve in Fig. 4b demonstrates a comparable fatigue performance to that of a rolled WE43 alloy in the low cycle fatigue regime described by Ghorbanpour et al. [43]. Both WE43 alloys exhibit moderate cyclic softening under cyclic loading. The ε-N curve was additionally supplemented with the data of an extruded WE43 alloy in the high cycle fatigue regime from Gu et al. [14], and the entire data set was correlated using the Manson–Coffin equation for predicting the fatigue life [44]:

$$\varepsilon_a = \varepsilon_a^e + \varepsilon_a^p = \frac{\sigma_f'}{E}(2N_f)^b + \varepsilon_f'(2N_f)^c \quad (2)$$

with the elastic modulus $E$, the fatigue strength coefficient $\sigma_f'$, the fatigue ductility coefficient $\varepsilon_f'$, the fatigue strength exponent b and the fatigue ductility exponent c. The total strain amplitude can be divided into an elastic $\varepsilon_a^e$ and a plastic $\varepsilon_a^p$ part. Table 1 provides an overview of the material parameters under static and dynamic test conditions. We determined the tensile properties using the engineering stress–strain curve from the tensile test. The yield strength and tensile strength were

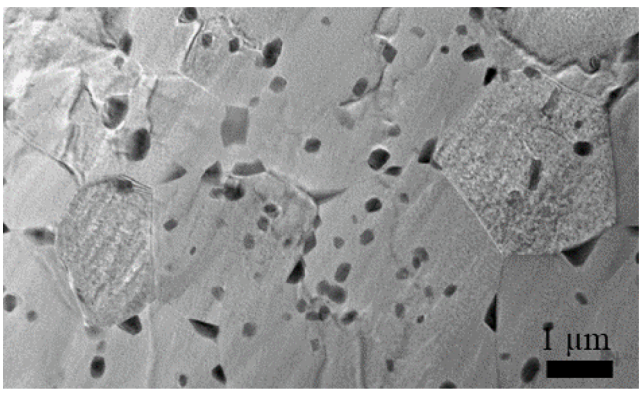


**Fig. 3.** TEM image of WE43 microstructure.

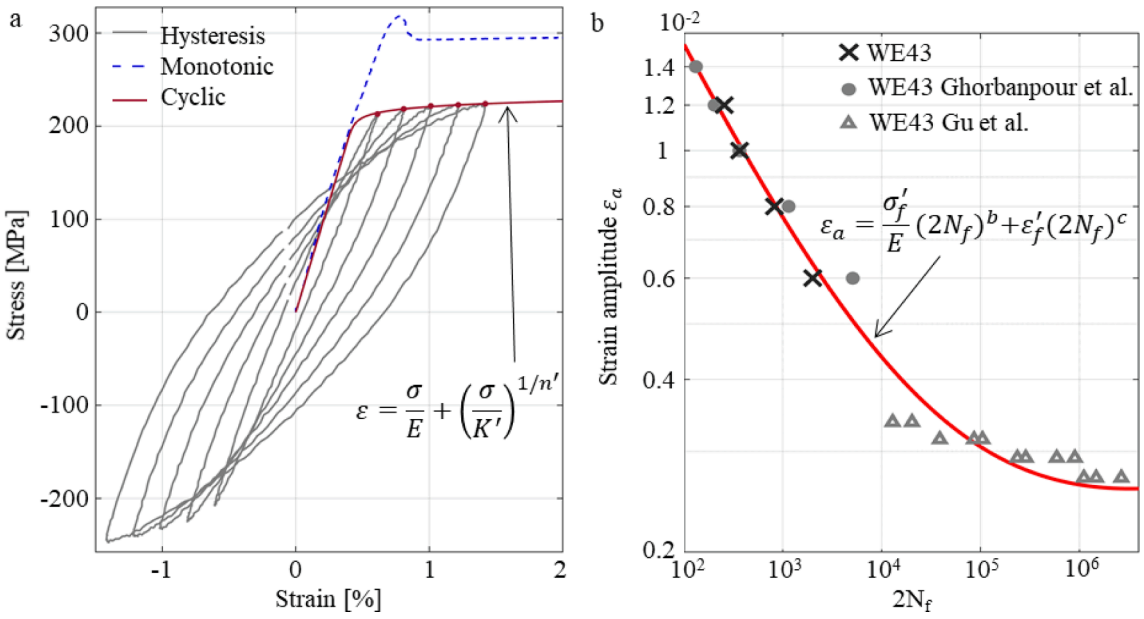


**Fig. 4.** (a) Cyclic stress–strain curve obtained from stabilised hysteresis loops of fully reversed (R= − 1) cyclic loadings with different strain amplitudes for alloy WE43. (b) Total strain amplitude versus reversals to failure $2N_f$ of WE43, supplemented with data from Ghorbanpour et al. [43] and Gu et al. [14].

**Table 1**
Static and dynamic material parameters of the WE43 alloy.

| Static material properties | | Fatigue properties | |
|---|---|---|---|
| Young's-Modulus E | 47.6 GPa | Ramberg-Osgood equation | |
| Yield strength $\sigma_y$ | 316 MPa | Cyclic strength coefficient K' | 252.15 MPa |
| Tensile strength $\sigma_m$ | 306 MPa | Cyclic hardening exponent n' | 0.02527 |
| Elongation-to-failure elongation $A_{gt}$ | 19.97 % | Manson-Coffin | |
| | | Fatigue strength coefficient $\sigma_f'$ | 42.92 MPa |
| | | Fatigue strength exponent b | 0.05741 |
| | | Fatigue ductility coefficient $\varepsilon_f'$ | 0.091 |
| | | Fatigue ductility exponent c | −0.352 |

calculated with the initial cross-section. The necking of the specimen was not accounted for in the engineering stress–strain curve. Therefore, the actual stress is underestimated at large plastic deformations, leading to a slightly higher yield strength compared to the tensile strength.

### 3.3. Stress–controlled corrosion-fatigue

The stress-fatigue life (S-N) curves of the WE43 alloy tested in air, after 1–day and 7–day precorrosion periods and in the corrosive environment are shown in Fig. 5. The relationship between the applied stress amplitude and the fatigue life above the fatigue limit is correlated using the Basquin equation [51]:

$$\sigma_A = A \times N_f^b \tag{3}$$

with the stress amplitude $\sigma_A$, the cycles to failure $N_f$, the coefficient A and the exponential factor b. The resulting material parameters for the different test conditions are presented in Table 2. The fatigue endurance of WE43 alloy in air at $2x10^6$ cycles is 99 MPa. Compared to the fatigue

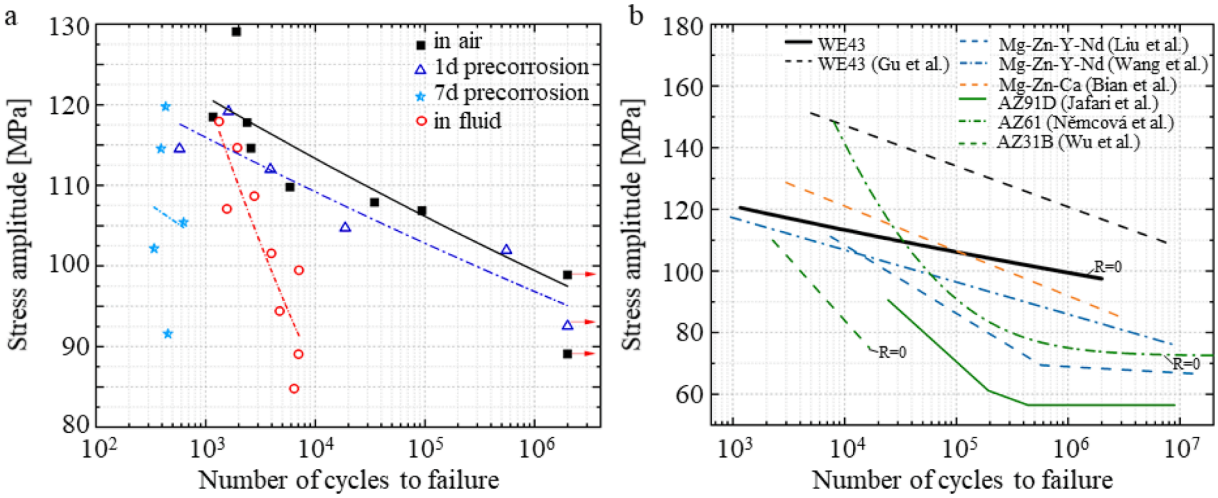


**Fig. 5.** (a) S-N curve of the WE43 alloy tested in air, in air after precorrosion of 1 or 7 days and in fluid. (b) Comparison of S-N curves of different alloy systems tested in air (Gu et al. [14], Liu et al. [45], Wang et al. [46], Bian et al. [47], Jafari et al. [48], Němcová et al. [49],Wu et al. [50]).

**Table 2**
Material parameters in the Basquin equation for different test conditions.

| Factor | Air | 1–day precorrosion | 7–day precorrosion | DMEM |
|---|---|---|---|---|
| A [MPa] | 147.24597 | 138.8379 | 134.03649 | 334.08618 |
| b | −0.02842 | −0.02608 | −0.03821 | −0.14625 |

behaviour of AZ31B tested in air with a stress ratio of R=0, WE43 exhibits a better fatigue performance, as shown in Fig. 5b. At $10^4$ cycles, WE43 has a fatigue strength of approximately 113 MPa and the AZ31B alloy of 84 MPa [50]. This can be attributed to changes in the microstructure due to alloying with rare-earth elements. Rare-earth elements act as grain refiner and form precipitates in the matrix. Both effects hinder deformation twinning and pin dislocation movement [52]. It is indicated that the magnesium alloy WE43 with rare-earth elements is more suitable for highly loaded orthopaedic implant systems. Cracks in fatigue experiments are initiated by internal defects that locally increase the stress concentration. After precorrosion, locally increased stresses at corrosion pits facilitate crack initiation. Hence, the precorroded specimens are expected to crack at preformed pits. However, in our previous work, we have concluded that the WE43 alloy corrodes rather non–homogeneously and is insensitive to pitting corrosion [40]. This insensitivity explains the rather small difference in fatigue performance between the non–corroded and 1–day pre–corroded alloy. The similar S–N curves show that the inhomogeneous corrosion front after 1–day precorrosion has no detrimental effect on the fatigue strength. The fatigue limit of the 1–day precorroded alloy, which is defined at $2x10^6$ cycles, is almost identical to the uncorroded alloy.

On the contrary, the progressing corrosion after 7 days in DMEM significantly deteriorates the fatigue performance. The advancing corrosion front leads to significant material dissolution, and fatigue failure occurs in less than $10^4$ cycles. Immersion tests with round specimens of 4 mm diameter have revealed inhomogeneous corrosion attack along the circumference. Almost uncorroded ridges and pits with the maximum depth of 440 μm were observed on the specimen's surface [40,41]. This inhomogeneous circumference, which includes a considerable number of corrosion pits with varying depth of up to 35 % of the specimen radius, leads to stress concentrations and local plastic deformations, which dramatically deteriorate the fatigue performance. The large scatter of the fatigue life after 7-day precorrosion may be attributed to the irregular corrosion front and randomly distributed corrosion pits. As a consequence, the Basquin model does not correlate the fatigue life of the heavily corroded specimens in an adequate manner.

In the CF tests in DMEM, mechanical loading and chemical attack strongly interact each other, leading to a significant change in the S–N curve of the WE43 specimens. The experimental results show that the number of cycles to failure at high stress amplitudes is similar to that of the uncorroded alloy. This confirms previous observations that the CF behaviour at high stress levels is predominantly influenced by the mechanical loading and the effect of the corrosion environment is relatively limited [35]. At lower stress levels, the fatigue life of the WE43 is significantly reduced, which can be explained by a longer immersion time in the corrosive medium and superimposed corrosion damage due to electrochemical processes [48]. Hence, the degradation of the fatigue performance depends on the material's corrosion properties [45]. It has been observed that the prolonged exposure to the corrosive environment is detrimental to fatigue [16,17]. On this account, a comparison of the CF resistance between different alloy systems as potential biodegradable implant material is not straightforward due to large variations in experimental conditions.

The detrimental effect of the corrosion environment on fatigue behaviour can be evaluated by the reduction ratio of fatigue strength (RRFS), which measures the reduction in fatigue strength due to the corrosion environment. To compare tests of different frequencies, we calculate here the reduction in fatigue strength in relation to a 2-hours cyclic loading inside the corrosion environment [60]:

$$RRFS = \left(\sigma_{air} - \sigma_{fluid}\right)/\sigma_{air} \quad (4)$$

with the stress amplitude in air $\sigma_{air}$ and the stress amplitude in fluid $\sigma_{fluid}$ after 2 h. Fig. 6a compares the relative reduction in fatigue strength RRSF of different magnesium alloys at the fatigue life that correspond to a cyclic loading of 2 h inside the corrosion environment. To the best knowledge of the authors, this is the first CF experiment using complex DMEM fluid, which is one of the most suitable media for in vitro corrosion studies as it is in closest in composition and concentration to human blood plasma [30].

After 2 h of cyclical loading in DMEM, the fatigue strength of the WE43 alloy is reduced by about 20 %. This value is higher than the results for Y- and Nd-containing magnesium alloys tested in SBF (WE43 and Mg-Zn-Y-Nd) [14,45,46]. However, it is noted that the larger maximum stresses and plastic deformations in the stress ratio case of our experiments may lead to a higher sensitivity of the fatigue performance to corrosive environments. Mg-Y-Zn and Mg-Zn-Zr show substantial reductions in the fatigue strength [17,53]. As both alloys contain either Y or Nd, this may indicate that to achieve favourable strength retention, alloying with both Y and Nd is required. Nd and Y are both present in WE43 and Mg-Zn-Y-Nd, with higher concentrations in WE43. The comparison between these two alloys reveals similar relative reductions in the fatigue strength, but the WE43 alloy is subjected to higher stress amplitude. It is suggested that the larger Y and Nd concentrations in WE43 contribute favourably to the high fatigue strength. The comparison also shows that the magnesium alloys containing aluminium or iron (AZ91D, AZ61, ZX10) do not outperform rare-earth alloy systems.

The effect of precorrosion on the fatigue performance of different magnesium alloys is compared in Fig. 6b. It is shown that the WE43 alloy has the highest fatigue life, even after 1-day of precorrosion. The aluminium-containing alloys exhibit a significantly lower fatigue performance. For longer precorrosion periods, the fatigue life of the rare-earth containing alloy ZEK100 decreases the least. The comparison shows that the magnesium alloy system can be tailored by the addition of rare-earth elements in order to achieve a suitable CF behaviour for medical applications.

Fig. 7 shows the stress–strain hysteresis of selected cycles of a fatigue test in air with the stress amplitude of 115 MPa and the fatigue life of 2,592 cycles. It is observed that the high stress amplitude in the low cycle fatigue regime results in an unstable stress–strain hysteresis with plastic ratchetting strain accumulating in each loading cycle. This ratcheting phenomenon has been reported for magnesium alloys and is related to twinning and dislocation slips [61]. The mean strain versus the normalised number of cycles is plotted in Fig. 8. At the initial stage, the mean strain increases rapidly. This rapid ratcheting rate then converts into a steady stage. The steady-ratcheting strain has been attributed to a balance between softening due to micro-crack development and strain hardening [13]. At the final fracture stage, the accumulated ratcheting strain dramatically increases again, leading to final failure. The comparison between different stress amplitudes shows that the ratchetting strain increases with higher stress amplitude and mean stress. This correlation has already been reported and linked to the increased density of twins at higher mean stress and stress amplitude [62–64]. The results within the two test groups of uncorroded and 1-day pre-corroded specimens show that the higher ratcheting strain leads to shorter fatigue life, which is consistent with reported results [59].

### 3.4. Fractography

Fig. 9 shows the fatigue fracture surfaces of the WE43 specimens under different loading conditions. Except the 7–day pre–corroded specimen tested with a low stress amplitude of 91.6 MPa, all fracture surfaces show three morphologically distinct zones: the crack initiation zone, the crack propagation zone and the overload zone. Additionally,

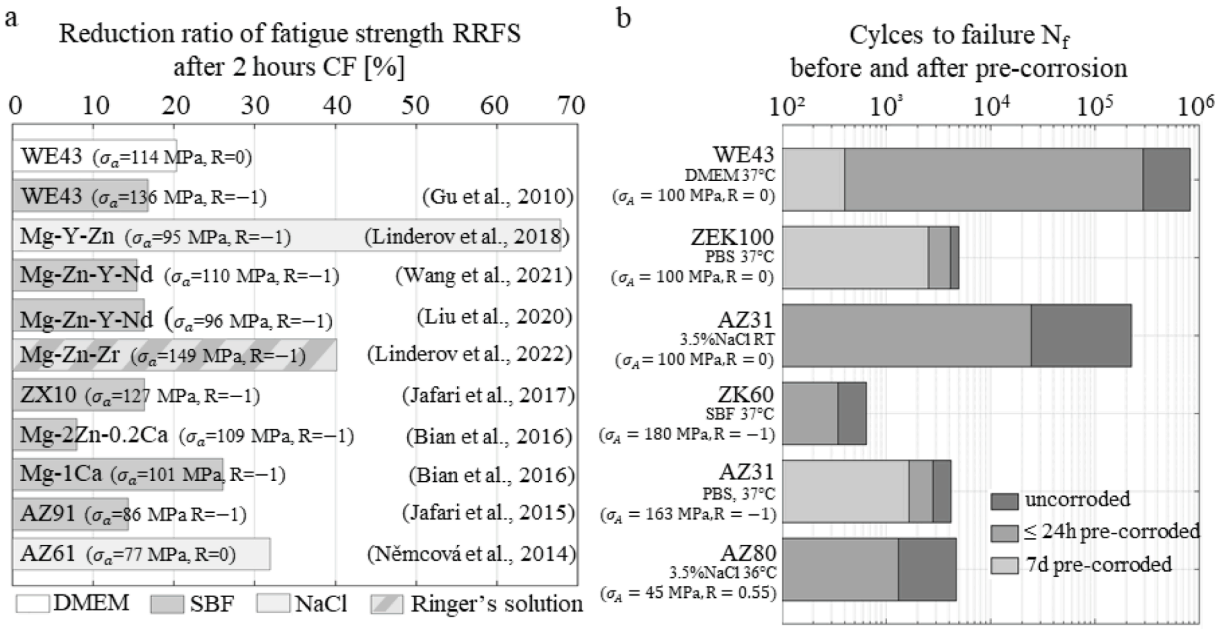


**Fig. 6.** (a) Comparison of relative reductions in the fatigue strength after 2h cyclic loadings in different corrosive environments for different magnesium alloy systems with corresponding stress amplitudes $\sigma_a$ (Gu et al. (2010) [14], Linderov et al. (2018) [53], Wang et al. (2021) [46], Liu et al. (2020) [45], Linderov et al. (2022) [17], Jafari et al. (2017) [54], Bian et al. (2016) [47], Jafari et al. (2015) [48], Němcová et al. (2014) [49]). (b) Comparison of the number of cycles to failure in air and after different precorrosion periods for different alloy systems (ZEK100 [55], AZ31 in NaCl [56], ZK60 [57], AZ31 in PBS [58], AZ80 [59]). Short pre-corrosion periods are 24 h for WE43 and AZ31 in PBS, 12 h for ZEK100, ZK60 and AZ80 and 3 h for AZ31 in NaCl.

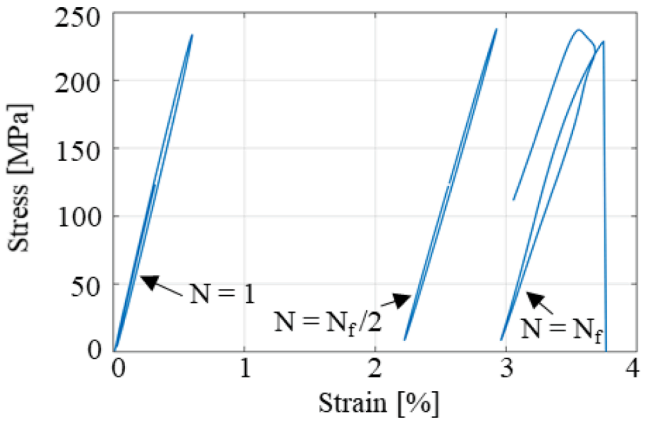


**Fig. 7.** Stress–strain loops at selected cycles of stress-controlled fatigue tests of WE43 in air with a stress amplitude of 115 MPa.

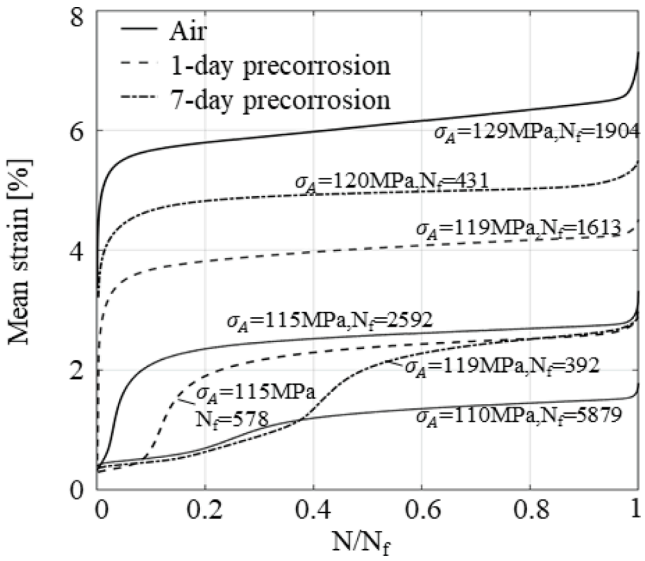


**Fig. 8.** Mean strain vs. normalised cycles during stress-controlled fatigue tests of WE43 in air in uncorroded state and after precorrosion.

shear lips are visible at the circumference. At lower stress amplitudes, the crack propagation zones are larger than at higher stress amplitudes, which corresponds to a larger number of cycles to failure.

SEM images of the three morphologically distinct zones of a WE43 specimen tested in air are presented in Fig. 10. Crack initiation in the uncorroded specimen, which is marked in Fig. 10a, cannot be clearly related to microstructural defects. In air, the fatigue source is related to surface or microstructural defects such as microcracks, micropores or inclusions [65,66]. In magnesium specimens free of defects, twin or slip boundary have also been reported as potential fatigue source, as they locally increase stress concentrations [61,67]. In the region near the crack initiation, as shown in Fig. 10b, striation marks are visible as well as transgranular cracking. A mixed mode has already been identified for the alloy in SCC conditions and has been observed in additively manufactured WE43 [41,68]. In the overload failure zone, we observe a dimple like morphology as shown in Fig. 10c.

### 3.4.1. *Fracture surfaces of pre-corroded specimens*

The crack initiation zone of the 1–day pre-corroded specimen, failing after 18,753 cycles at a stress amplitude of 105 MPa (specimen shown in Fig. 9f), is shown at a higher magnification in Fig. 11a. Corrosion products are clearly visible on the specimen circumference. Localised corrosion but no severe corrosion pits can be identified. Hence, crack initiation might not be related to an increased stress concentration at a deep pit for the 1–day pre–corroded group. The SEM image shows cracks in the corrosion products that have propagated throughout the thickness of the passive layer. At the interface of a brittle material and ductile metallic substrate, cracks can easily form inside the brittle material due to differing elastic properties. Due to the high stress concentration at the

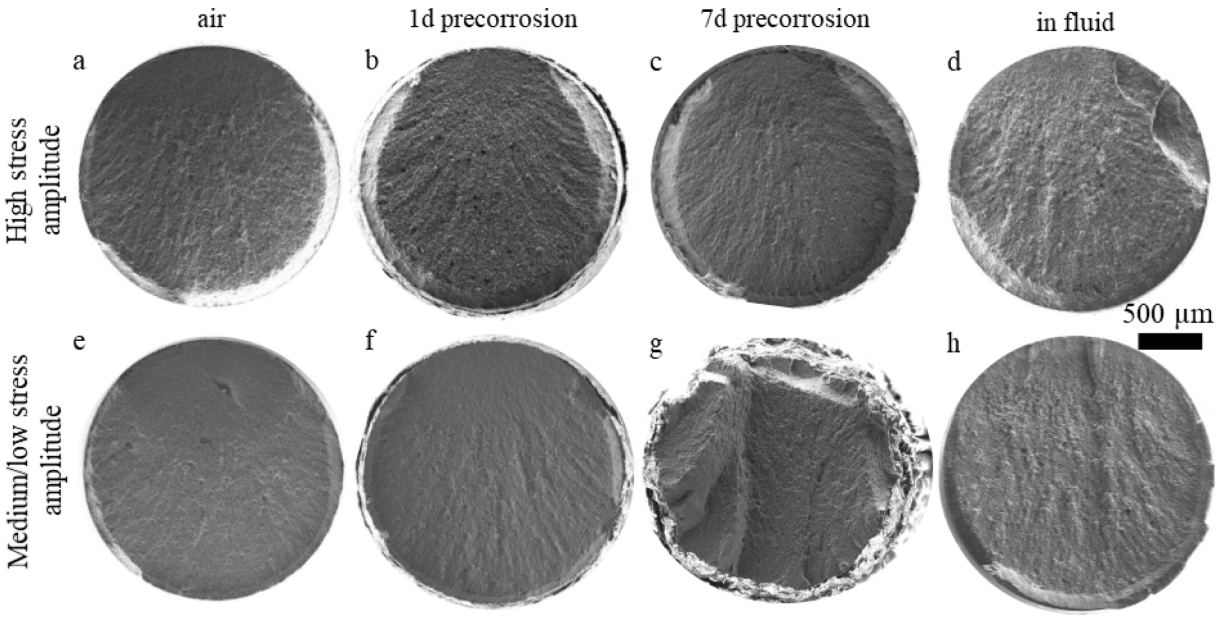


**Fig. 9.** Fracture surfaces of WE43 specimens cyclically loaded in air, in air after precorrosion for 1 or 7 days in DMEM or in DMEM.

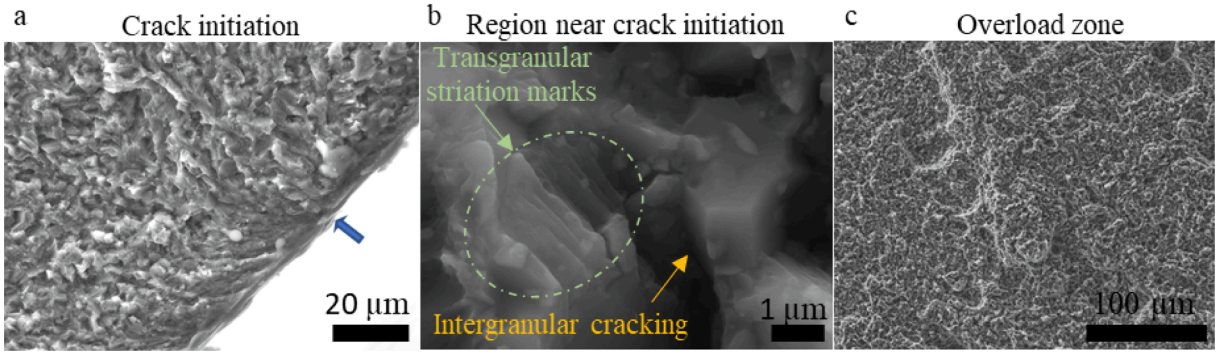


**Fig. 10.** SEM images for details of fracture surfaces. (a) Crack initiation site (marked with blue arrow) of an uncorroded specimen failing after $9.3x10^4$ cycles in air (in Fig. 9e). (b) Crack propagation zone of 1-day pre-corroded specimen (in Fig. 9b) with evidence of inter- and transgranular cracking. (c) Evidence of dimple formation in overload zone of uncorroded specimen (in Fig. 9e). (For interpretation of the references to colour in this figure legend, the reader is referred to the web version of this article.)

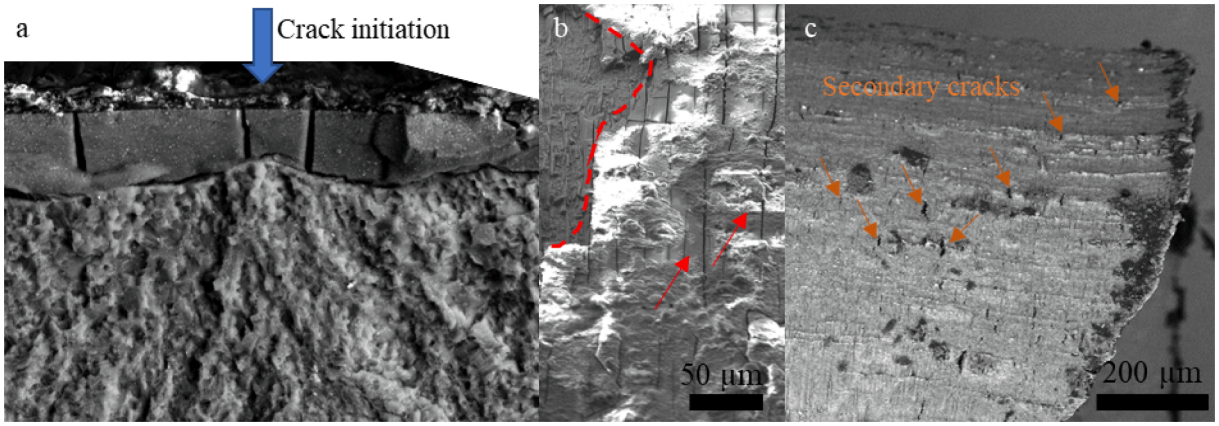


**Fig. 11.** (a) BSE SEM image of crack initiation zone of 1-day pre-corroded specimen (inFig. 9 f). (b) Side view of 1-day pre-corroded specimen (in Fig. 9b) with the evidence of corrosion product cracking (highlighted by arrows) and evidence of corrosion product exfoliation (area highlighted with dashed line). (c) Side view close to fatigue fracture of 1-day pre-corroded specimen (in Fig. 9b) with the evidence of secondary cracks (highlighted by arrows).

crack tip, the crack can easily propagate into the metallic substrate and initiate fatigue failure of the alloy [69,70]. Crack formation at the interface between the oxide layer and the alloy has already been observed in an AZ91D alloy after straining in organic solution [29]. Such cracks can serve as additional CF sources and result in lower cycles-to-failure despite the lower measured ratcheting strain in the 1-day pre–corroded group, compared to the uncorroded specimen group.

Fig. 11b and c show the side view of the pre-corroded specimen after fatigue failure. A layer of corrosion products is visible on the surface that is traversed by a dense network of aligned secondary cracks (marked by red arrows), which confirms the intensive cracking of the passive layer under cyclic loadings. The side view also shows regions with exfoliated corrosion products (marked in red), which usually appear at larger strains due to a mismatch of elastic properties between surface layer and substrate. At the circumference close to the fatigue fracture, the corrosion products have almost entirely exfoliated, revealing secondary cracks on the circumference of the specimen. These cracks are rather short but aligned perpendicular to the loading direction and are usually associated with local material embrittlement [71]. The embrittlement is caused by the absorption of hydrogen by the magnesium matrix during the preceding exposure to the corrosion environment. The cracks on the circumference seen in Fig. 11c might have developed from microcracks that formed in the brittle corrosion product layer. Crack propagation into the metallic substrate leads to high stress concentrations at the crack tip and can trigger hydrogen embrittlement during the post-exposure straining [72]. The hydrogen accumulates at locations of high stresses and weakens the atomic bonds. Preimmersion in an aggressive corrosion environment has shown to increase the hydrogen concentration [71]. Hence, the secondary cracks are attributed to a combination of crack propagation from the corrosion products and hydrogen embrittlement.

A prolonged precorrosion period of 7 days has a significant detrimental effect on the fatigue life of the alloy, which can be confirmed by characteristics in the fracture surface of the specimen loaded with a stress amplitude of 92 MPa (see Fig. 9g). The SEM image shows multiple shear lips as crack initiation zones. As analysed in previous studies, 7 days of precorrosion can cause localised corrosion damage, forming pits of about 230 μm in DMEM and about 150 μm in c–SBF [39,40], which is sufficient to locally increase the stress concentration, facilitating crack initiation [73]. In addition, the hydrogen concentration in the magnesium substrate may increase due to the prolonged exposure time to the corrosion environment, leading to a high degree of material embrittlement [71]. Moreover, a passive layer up to 220 μm in thickness can form after 7 days immersion time in DMEM. As a result, larger cracks can form within the passive layer, which can propagate into the magnesium alloy substrate, accelerating the propagation of fatigue cracks in magnesium substrate. Very few secondary cracks of up to 170 μm were observed in the side view.

### 3.4.2. *Fracture surfaces of corrosion-fatigue specimens*

In the CF experiments, several shear lips can be observed in the specimens loaded in DMEM with high stress amplitudes, which are more pronounced, as shown in Fig. 9d. The crack initiation zone of the specimen loaded with a stress amplitude of 102 MPa (see Fig. 9h) is presented in more detail in Fig. 12a. Close to the fatigue source, the fracture is covered by a thin layer of corrosion products and a distinct layer is visible on the circumference distant from the crack initiation zone, as shown in Fig. 12b. This is a clear indication of simultaneous deformation and corrosion processes. When the alloy is exposed to the corrosive environment, microgalvanic corrosion occurs, leading to localised corrosion attack and the release of atomic hydrogen [38]. In a static corrosion environment, the dissolution of the magnesium matrix would be decelerated by the formation of a protective oxide layer. In contrast, the corrosion process is accelerated by the stress-induced passive layer breakdown under cyclic loading [28]. In addition, the stress-assisted hydrogen absorption and dissolution of the magnesium matrix can lead to increased corrosion rates [74,75]. These deteriorative mechanisms become evident through a large number of stress corrosion cracks on the circumference, which are of several hundred micrometres in length, as shown in Fig. 12c [41,71,76,77]. All of the above mechanisms mutually interact and take place repetitively, resulting in a significant shorter fatigue life in the CF experiments.

With increased exposure time to the corrosion environment, the formation of fatigue source is facilitated due to environmentally assisted mechanisms. The corrosion processes are more dominant at low stress amplitudes with a higher number of cycles-to-failure. At high stress amplitudes, the fatigue damage is mainly attributed to the mechanical loadings. Since the CF is an intrinsic time-dependent process, the test frequency of magnesium alloys for biomedical applications should be in the physiological regime. Another important factor is the physiological chloride concentration of the fluid, as high concentration of chlorides increases susceptibility to stress corrosion cracking [78].

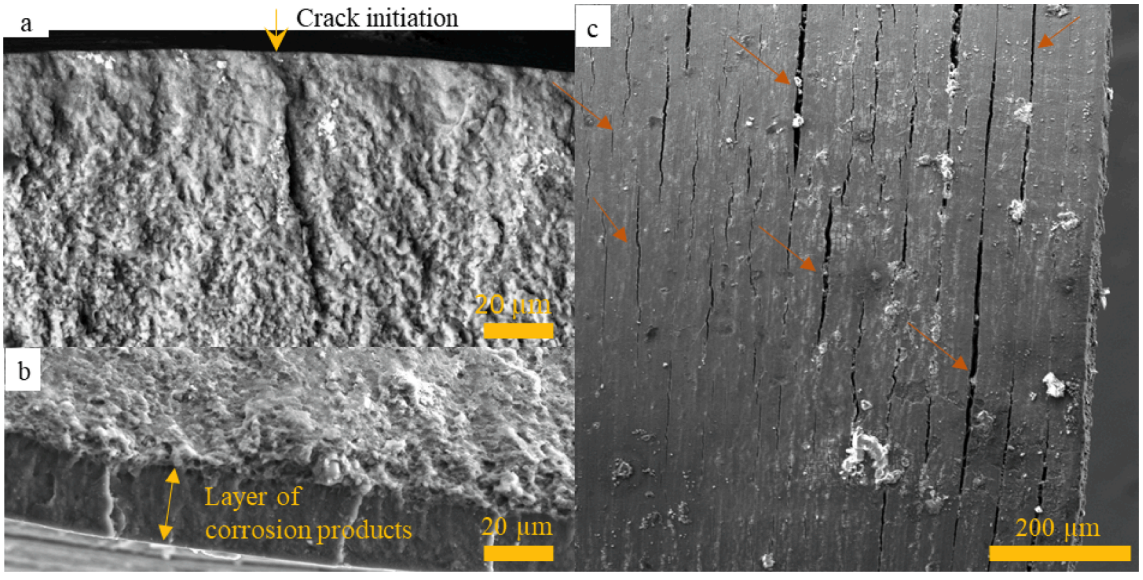


**Fig. 12.** SEM images of specimen dynamically loaded in the corrosion fluid (in Fig. 9h). (a) BSE SEM image of crack initiation zone. (b) BSE SEM image distant from crack initiation zone. (c) Side view close to fatigue fracture with evidence of secondary cracks (highlighted by arrows).

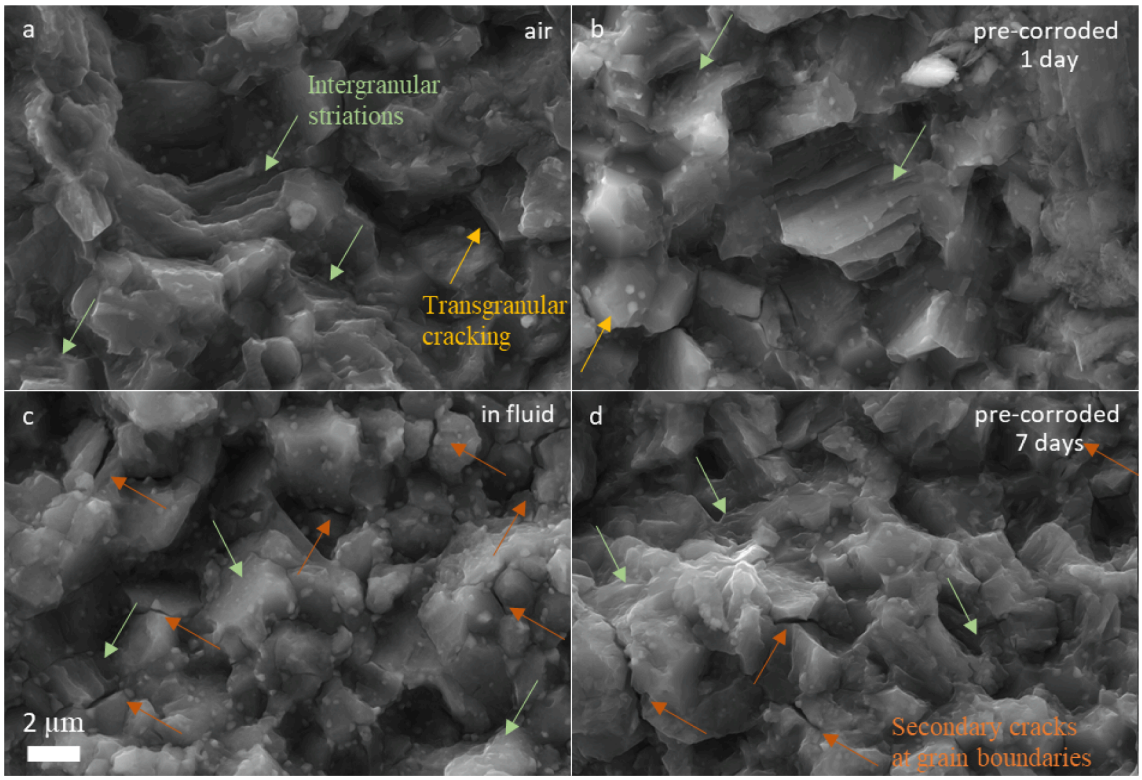


**Fig. 13.** SEM image of crack growth regions of WE43 specimen of different test conditions. (a) Uncorroded specimen. (b) 1-day pre-corroded specimen. (c) Specimen loaded in fluid. (d) 7-day pre-corroded specimen. Scale bar applies for all images. Intergranular cracking indicated by green arrow, transgranular cracking indicated by yellow arrow, and secondary cracks at grain boundaries indicated by orange arrow. (For interpretation of the references to colour in this figure legend, the reader is referred to the web version of this article.)

Fig. 13 shows SEM images of the crack propagation zone of the four different test configurations at high magnification. All specimens show a mixed mode of intergranular cracking with striation marks and transgranular cracking, but significant differences in the predominant modes are visible. In uncorroded state, transgranular cracking is predominant. Interestingly, we observe less striation marks, more intergranular cracking and more secondary cracks along grain boundaries in the longer pre-corroded specimen and in the specimen loaded inside the fluid. The intergranular mode even prevails in CF configuration. This may be an indicator for the presence of hydrogen assisted mechanisms that weaken the bonds between grains and lead to more crack branching. In aluminium-containing magnesium alloys, cleavage or transgranular fracture was identified as the prevalent fracture mode in CF experiments [48,49]. The same applies to these alloys in fatigue tests after precorrosion, with no significant changes in the failure modes reported after precorrosion [56,79]. In the aluminium-free alloy ZK60, intergranular brittle fracture patterns and secondary cracks were observed in CF. The differences in the prevalent failure mode between the uncorroded, the precorroded and the specimens tested in fluid shows, that the failure mode of the WE43 alloy strongly depends on the experimental fatigue configuration. The failure mode changes after precorrosion and is dependent on the precorrosion period as well as on the cyclical loading in the corrosive environment.

## 4. Conclusions

In the present study, we analysed the corrosion-fatigue behaviour of a medical-grade magnesium alloy WE43MEO containing rare-earth elements. A cell culture fluid containing organic compounds (DMEM) was used for the physiological test conditions. To overcome the experimental limitations arising from the susceptibility of the fluid to contamination, sterile test conditions were employed. Finally, fracture surfaces were analysed using scanning electron microscopy. Based on the experimental results, the following conclusion can be drawn:

- The WE43 alloy exhibits cyclic softening in air with a fatigue limit of 99 MPa at $2x10^6$ cycles. The ratcheting strain tends to be higher with increasing stress amplitudes.
- Compared to the effect of 1-day precorrosion on the fatigue life, 7-day precorrosion significantly deteriorated the fatigue performance, independent of the stress amplitude. This can be attributed to large secondary cracks potentially induced by hydrogen embrittlement, which formed perpendicular to the loading direction during cyclic loadings. These cracks developed either from corrosion pits or from cracks that formed in the brittle corrosion product layer and propagated into the magnesium matrix.
- In the corrosion-fatigue tests in the organic fluid, the fatigue life was considerably reduced due to continuous exposure to the corrosive environment. This particularly applied for small stress amplitudes. The corrosion-fatigue strength was 85 MPa at $8x10^3$ cycles.
- Stress corrosion mechanisms generally reduce fatigue life of bioabsorbable magnesium alloys. The present results on WE43 fatigue life testing in DMEM confirm this behaviour. Clear signs of environmentally assisted cracking are visible on the specimen's circumference. A significant number of long and aligned secondary cracks indicate material embrittlement.

Fractography reveals three distinct regions: crack initiation zone, crack propagation zone and overload zone. In corrosion-fatigue experiments, the initiation of the fatigue source is linked to corrosion pits, with secondary cracks forming along the circumference. In the crack propagation zone, all specimens showed mixed modes of intergranular and transgranular cracking. However, the predominant failure mode strongly depends on the experimental fatigue configuration.

Transgranular cracking was dominant in uncorroded states, while the transition to intergranular cracking dominant failure was observed in corrosion-fatigue tests due to hydrogen embrittlement.

## CRediT authorship contribution statement

**Julia Nachtsheim:** Writing – original draft, Visualization, Validation, Methodology, Investigation, Data curation, Conceptualization. **Songyun Ma:** Writing – review & editing, Visualization, Validation, Supervision, Project administration, Methodology, Investigation, Funding acquisition, Formal analysis, Conceptualization. **Jaka Burja:** Writing – review & editing, Visualization, Methodology, Investigation. **Alexander Kopp:** Resources, Formal analysis. **Jan-Marten Seitz:** Resources, Formal analysis. **Bernd Markert:** Writing – review & editing, Supervision, Resources.

## Declaration of competing interest

The authors declare that they have no known competing financial interests or personal relationships that could have appeared to influence the work reported in this paper.

## Data availability

Data will be made available on request.

## Acknowledgement

This research was supported by the German Ministry of Education and Research (13GW0352B). The authors would like to thank Barbara Šentina Batič for assistance with SEM images, Borut Žužek for material analysis and Dongxu Liu, Laurent Schartz, Mario Hackbarth and Uwe Navrath for support with the fatigue experiments.

## References

[1] Castellani C, Lindtner RA, Hausbrandt P, Tschegg E, Stanzl-Tschegg SE, Zanoni G, et al. Bone-implant interface strength and osseointegration: Biodegradable magnesium alloy versus standard titanium control. Acta Biomater 2011;7:432–40. https://doi.org/10.1016/j.actbio.2010.08.020.

[2] Liu J, Liu B, Min S, Yin B, Peng B, Yu Z, et al. Biodegradable magnesium alloy WE43 porous scaffolds fabricated by laser powder bed fusion for orthopedic applications: Process optimization, in vitro and in vivo investigation. Bioact Mater 2022;16:301–19. https://doi.org/10.1016/j.bioactmat.2022.02.020.

[3] Rendenbach C, Fischer H, Kopp A, Schmidt-Bleek K, Kreiker H, Stumpp S, et al. Improved in vivo osseointegration and degradation behavior of PEO surface-modified WE43 magnesium plates and screws after 6 and 12 months. Mater Sci Eng C 2021;129. https://doi.org/10.1016/j.msec.2021.112380.

[4] Feyerabend F, Fischer J, Holtz J, Witte F, Willumeit R, Drücker H, et al. Evaluation of short-term effects of rare earth and other elements used in magnesium alloys on primary cells and cell lines. Acta Biomater 2010;6:1834–42. https://doi.org/10.1016/j.actbio.2009.09.024.

[5] Dey M, Singh RK. Neurotoxic effects of aluminium exposure as a potential risk factor for Alzheimer's disease. Pharmacol Rep 2022;74:439–50. https://doi.org/10.1007/s43440-022-00353-4.

[6] Darbre PD, Mannello F, Exley C. Aluminium and breast cancer: Sources of exposure, tissue measurements and mechanisms of toxicological actions on breast biology. J Inorg Biochem 2013;128:257–61. https://doi.org/10.1016/j.jinorgbio.2013.07.005.

[7] Witte F, Kaese V, Haferkamp H, Switzer E, Meyer-Lindenberg A, Wirth CJ, et al. In vivo corrosion of four magnesium alloys and the associated bone response. Biomaterials 2005;26:3557–63. https://doi.org/10.1016/j.biomaterials.2004.09.049.

[8] Weng W, Biesiekierski A, Li Y, Dargusch M, Wen C. A review of the physiological impact of rare earth elements and their uses in biomedical Mg alloys. Acta Biomater 2021;130:80–97. https://doi.org/10.1016/j.actbio.2021.06.004.

[9] Choudhary L, Raman RKS, Hofstetter J, Uggowitzer PJ. In-vitro characterization of stress corrosion cracking of aluminium-free magnesium alloys for temporary bio-implant applications. Mater Sci Eng C 2014;42:629–36. https://doi.org/10.1016/j.msec.2014.06.018.

[10] Singh Raman RK, Jafari S, Harandi SE. Corrosion fatigue fracture of magnesium alloys in bioimplant applications: A review. Eng Fract Mech 2015;137:97–108. https://doi.org/10.1016/j.engfracmech.2014.08.009.

[11] Zan R, Shen S, Huang Y, Yu H, Liu Y, Yang S, et al. Research hotspots and trends of biodegradable magnesium and its alloys. Smart Mater Med 2023;4:468–79. https://doi.org/10.1016/j.smaim.2023.01.002.

[12] Olugbade TO, Omiyale BO, Ojo OT. Corrosion, Corrosion Fatigue, and Protection of Magnesium Alloys: Mechanisms, Measurements, and Mitigation. J Mater Eng Perform 2022;31:1707–27. https://doi.org/10.1007/s11665-021-06355-2.

[13] Chen G, Lu LT, Cui Y, Xing RS, Gao H, Chen X. Ratcheting and low-cycle fatigue characterizations of extruded AZ31B Mg alloy with and without corrosive environment. Int J Fatigue 2015;80:364–71. https://doi.org/10.1016/j.ijfatigue.2015.06.022.

[14] Gu XN, Zhou WR, Zheng YF, Cheng Y, Wei SC, Zhong SP, et al. Corrosion fatigue behaviors of two biomedical Mg alloys - AZ91D and WE43 - In simulated body fluid. Acta Biomater 2010;6:4605–13. https://doi.org/10.1016/j.actbio.2010.07.026.

[15] Wang BJ, Xu DK, Wang SD, Sheng LY, Zeng RC, Hou Han E. Influence of solution treatment on the corrosion fatigue behavior of an as-forged Mg-Zn-Y-Zr alloy. Int J Fatigue 2019;120:46–55. https://doi.org/10.1016/j.ijfatigue.2018.10.019.

[16] Wegner N, Kotzem D, Wessarges Y, Emminghaus N, Hoff C, Tenkamp J, et al. Corrosion and corrosion fatigue properties of additively manufactured magnesium alloy WE43 in comparison to titanium alloy Ti-6Al-4V in physiological environment. Materials 2019;12. https://doi.org/10.3390/ma12182892.

[17] Linderov M, Brilevsky A, Merson D, Danyuk A, Vinogradov A. On the Corrosion Fatigue of Magnesium Alloys Aimed at Biomedical Applications: New Insights from the Influence of Testing Frequency and Surface Modification of the Alloy ZK60. Materials 2022;15. https://doi.org/10.3390/ma15020567.

[18] Mei D, Lamaka SV, Gonzalez J, Feyerabend F, Willumeit-Römer R, Zheludkevich ML. The role of individual components of simulated body fluid on the corrosion behavior of commercially pure Mg. Corros Sci 2019;147:81–93. https://doi.org/10.1016/j.corsci.2018.11.011.

[19] Zhao MC, Liu M, Song GL, Atrens A. Influence of pH and chloride ion concentration on the corrosion of Mg alloy ZE41. Corros Sci 2008;50:3168–78. https://doi.org/10.1016/j.corsci.2008.08.023.

[20] Xin Y, Huo K, Tao H, Tang G, Chu PK. Influence of aggressive ions on the degradation behavior of biomedical magnesium alloy in physiological environment. Acta Biomater 2008;4:2008–15. https://doi.org/10.1016/j.actbio.2008.05.014.

[21] Zeng RC, Hu Y, Guan SK, Cui HZ, Han EH. Corrosion of magnesium alloy AZ31: The influence of bicarbonate, sulphate, hydrogen phosphate and dihydrogen phosphate ions in saline solution. Corros Sci 2014;86:171–82. https://doi.org/10.1016/j.corsci.2014.05.006.

[22] Johnston S, Dargusch M, Atrens A. Building towards a standardised approach to biocorrosion studies: a review of factors influencing Mg corrosion in vitro pertinent to in vivo corrosion. Sci China Mater 2018;61:475–500. https://doi.org/10.1007/s40843-017-9173-7.

[23] Mei D, Lamaka SV, Feiler C, Zheludkevich ML. The effect of small-molecule bio-relevant organic components at low concentration on the corrosion of commercially pure Mg and Mg-0.8Ca alloy: An overall perspective. Corros Sci 2019;153:258–71. https://doi.org/10.1016/j.corsci.2019.03.039.

[24] Xin Y, Hu T, Chu PK. Influence of Test Solutions on In Vitro Studies of Biomedical Magnesium Alloys. J Electrochem Soc 2010;157:C238. https://doi.org/10.1149/1.3421651.

[25] Törne K, Örnberg A, Weissenrieder J. The influence of buffer system and biological fluids on the degradation of magnesium. J Biomed Mater Res B Appl Biomater 2017;105:1490–502. https://doi.org/10.1002/jbm.b.33685.

[26] Xin Y, Chu PK. Influence of Tris in simulated body fluid on degradation behavior of pure magnesium. Mater Chem Phys 2010;124:33–5. https://doi.org/10.1016/j.matchemphys.2010.07.010.

[27] Kannan MB, Khakbaz H, Yamamoto A. Understanding the influence of HEPES buffer concentration on the biodegradation of pure magnesium: An electrochemical study. Mater Chem Phys 2017;197:47–56. https://doi.org/10.1016/j.matchemphys.2017.05.024.

[28] Meng Y, Gao H, Hu J, Gao L. Effect of pH value on the corrosion and corrosion fatigue behavior of AM60 magnesium alloy. J Mater Res 2019;34:1054–63. https://doi.org/10.1557/jmr.2018.489.

[29] Harandi SE, Banerjee PC, Easton CD, Raman RKS. Influence of bovine serum albumin in Hanks' solution on the corrosion and stress corrosion cracking of a magnesium alloy. Mater Sci Eng C 2017;80:335–45. https://doi.org/10.1016/j.msec.2017.06.002.

[30] Hou RQ, Scharnagl N, Willumeit-Römer R, Feyerabend F. Different effects of single protein vs. protein mixtures on magnesium degradation under cell culture conditions. Acta Biomater 2019;98:256–68. https://doi.org/10.1016/j.actbio.2019.02.013.

[31] Höhlinger M, Christa D, Zimmermann V, Heise S, Boccaccini AR, Virtanen S. Influence of proteins on the corrosion behavior of a chitosan-bioactive glass coated magnesium alloy. Mater Sci Eng C 2019;100:706–14. https://doi.org/10.1016/j.msec.2019.02.034.

[32] Yamamoto A, Hiromoto S. Effect of inorganic salts, amino acids and proteins on the degradation of pure magnesium in vitro. Mater Sci Eng C 2009;29:1559–68. https://doi.org/10.1016/j.msec.2008.12.015.

[33] Mei D, Lamaka SV, Lu X, Zheludkevich ML. Selecting medium for corrosion testing of bioabsorbable magnesium and other metals – A critical review. Corros Sci 2020;171. https://doi.org/10.1016/j.corsci.2020.108722.

[34] Chen L, Blawert C, Yang J, Hou R, Wang X, Zheludkevich ML, et al. The stress corrosion cracking behaviour of biomedical Mg-1Zn alloy in synthetic or natural biological media. Corros Sci 2020;175. https://doi.org/10.1016/j.corsci.2020.108876.

[35] Harandi SE, Singh Raman RK. Corrosion fatigue of a magnesium alloy under appropriate human physiological conditions for bio-implant applications. Eng Fract Mech 2017;186:134–42. https://doi.org/10.1016/j.engfracmech.2017.09.031.
[36] J. Zhou, E. Georgas, Y. Su, J. Zhou, N. Kröger, F. Benn, A. Kopp, Y.X. Qin, D. Zhu, Evolution from Bioinert to Bioresorbable: In Vivo Comparative Study of Additively Manufactured Metal Bone Scaffolds, Advanced Science 10 (2023). Doi: 10.1002/advs.202302702.
[37] Benn F, Kröger N, Zinser M, van Gaalen K, Vaughan TJ, Yan M, et al. Influence of surface condition on the degradation behaviour and biocompatibility of additively manufactured WE43. Mater Sci Eng C 2021;124. https://doi.org/10.1016/j.msec.2021.112016.
[38] Nachtsheim J, Ma S, Burja J, Batič BŠ, Markert B. Tuning the long-term corrosion behaviour of biodegradable WE43 magnesium alloy by PEO coating. Surf Coat Technol 2023;474:130115. https://doi.org/10.1016/j.surfcoat.2023.130115.
[39] van Gaalen K, Quinn C, Weiler M, Gremse F, Benn F, McHugh PE, et al. Predicting localised corrosion and mechanical performance of a PEO surface modified rare earth magnesium alloy for implant use through in-silico modelling. Bioact Mater 2023;26:437–51. https://doi.org/10.1016/j.bioactmat.2023.03.009.
[40] Nachtsheim J, Burja J, Ma S, Markert B. Long-Term in Vitro Corrosion of Biodegradable WE43 Magnesium Alloy in DMEM. Metals (Basel) 2022;12. https://doi.org/10.3390/met12122062.
[41] Nachtsheim J, Ma S, Burja J, Markert B. In vitro evaluation of stress corrosion cracking susceptibility of PEO-coated rare-earth magnesium alloy WE43. Surf Coat Technol 2024;477. https://doi.org/10.1016/j.surfcoat.2024.130391.
[42] Mei T, Wang Q, Liu M, Jiang Y, Zou T, Cai Y. The Low-Cycle Fatigue Behavior, Microstructure Evolution, and Life Prediction of SS304: Influence of Temperature. Materials 2023;16. https://doi.org/10.3390/ma16186326.
[43] Ghorbanpour S, McWilliams BA, Knezevic M. Low-cycle fatigue behavior of rolled WE43-T5 magnesium alloy. Fatigue Fract Eng Mater Struct 2019;42:1357–72. https://doi.org/10.1111/ffe.12992.
[44] Ma S, Markert B, Yuan H. Multiaxial fatigue life assessment of sintered porous iron under proportional and non-proportional loadings. Int J Fatigue 2017;97:214–26. https://doi.org/10.1016/j.ijfatigue.2017.01.005.
[45] Liu M, Wang J, Zhu S, Zhang Y, Sun Y, Wang L, et al. Corrosion fatigue of the extruded Mg–Zn–Y–Nd alloy in simulated body fluid. J Magnesium Alloys 2020;8:231–40. https://doi.org/10.1016/j.jma.2019.09.009.
[46] Wang J, Wang J, Fu Q, Sheng K, Liu M, Sun Y, et al. Microstructure, mechanical properties and corrosion fatigue behaviour of biodegradable Mg–Zn–Y–Nd alloy prepared by double extrusion. Corros Eng Sci Technol 2021;56:584–93. https://doi.org/10.1080/1478422X.2021.1923178.
[47] Bian D, Zhou W, Liu Y, Li N, Zheng Y, Sun Z. Fatigue behaviors of HP-Mg, Mg–Ca and Mg–Zn–Ca biodegradable metals in air and simulated body fluid. Acta Biomater 2016;41:351–60. https://doi.org/10.1016/j.actbio.2016.05.031.
[48] Jafari S, Singh Raman RK, Davies CHJ. Corrosion fatigue of a magnesium alloy in modified simulated body fluid. Eng Fract Mech 2015;137:2–11. https://doi.org/10.1016/j.engfracmech.2014.07.007.
[49] Němcová A, Skeldon P, Thompson GE, Morse S, Čížek J, Pacal B. Influence of plasma electrolytic oxidation on fatigue performance of AZ61 magnesium alloy. Corros Sci 2014;82:58–66. https://doi.org/10.1016/j.corsci.2013.12.019.
[50] Wu B, Song L, Duan G, Du X, Wang Y, Esling C, et al. Effect of cyclic frequency on uniaxial ratcheting behavior of a textured AZ31B magnesium alloy under stress control. Mater Sci Eng A 2020;795. https://doi.org/10.1016/j.msea.2020.139675.
[51] O.H. Basquin, The experimental law of endurance tests, in: Proc. AsTM, 1969: p. 625.
[52] Mirza FA, Chen DL. Fatigue of rare-earth containing magnesium alloys: A review. Fatigue Fract Eng Mater Struct 2014;37:831–53. https://doi.org/10.1111/ffe.12198.
[53] Linderov M, Vasilev E, Merson D, Markushev M, Vinogradov A. Corrosion fatigue of fine grain Mg-Zn-Zr and Mg-Y-Zn alloys. Metals (Basel) 2018;8. https://doi.org/10.3390/met8010020.
[54] Jafari S, Raman RKS, Davies CHJ, Hofstetter J, Uggowitzer PJ, Löffler JF. Stress corrosion cracking and corrosion fatigue characterisation of MgZn1Ca0.3 (ZX10) in a simulated physiological environment. J Mech Behav Biomed Mater 2017;65:634–43. https://doi.org/10.1016/j.jmbbm.2016.09.033.
[55] Zhao J, Gao LL, Gao H, Yuan X, Chen X. Biodegradable behaviour and fatigue life of ZEK100 magnesium alloy in simulated physiological environment. Fatigue Fract Eng Mater Struct 2015;38:904–13. https://doi.org/10.1111/ffe.12262.
[56] Bahmanabadi H, Shamsarjmand M. Modeling of fatigue behavior in pre-corroded AZ31 magnesium alloy. Forces in Mechanics 2024;14. https://doi.org/10.1016/j.finmec.2023.100254.
[57] Xiong Y, Yu Y, Hu X. Fatigue behavior of modified ZK60 magnesium alloy after pre-corrosion under stress-controlled loading. Eng Fract Mech 2022;260. https://doi.org/10.1016/j.engfracmech.2021.108187.
[58] Fu S, Gao H, Chen G, Gao L, Chen X. Deterioration of mechanical properties for pre-corroded AZ31 sheet in simulated physiological environment. Mater Sci Eng A 2014;593:153–62. https://doi.org/10.1016/j.msea.2013.11.012.
[59] Xiong Y, He L. Ratcheting behavior of surface-modified AZ80 magnesium alloy after pre-corrosion in simulated body fluids with various pH values. Fatigue Fract Eng Mater Struct 2023;46:4729–42. https://doi.org/10.1111/ffe.14157.
[60] Bhuiyan MS, Mutoh Y, Murai T, Iwakami S. Corrosion fatigue behavior of extruded magnesium alloy AZ61 under three different corrosive environments. Int J Fatigue 2008;30:1756–65. https://doi.org/10.1016/j.ijfatigue.2008.02.012.
[61] Wang Z, Wu S, Lei Y, Kan Q, Kang G. Damage evolution of extruded magnesium alloy from deformation twinning and dislocation slipping in uniaxial stress-controlled low cycle fatigue. Int J Fatigue 2022;164. https://doi.org/10.1016/j.ijfatigue.2022.107124.
[62] Lin YC, Liu ZH, Chen XM, Chen J. Uniaxial ratcheting and fatigue failure behaviors of hot-rolled AZ31B magnesium alloy under asymmetrical cyclic stress-controlled loadings. Mater Sci Eng A 2013;573:234–44. https://doi.org/10.1016/j.msea.2013.03.004.
[63] Lin YC, Chen XM, Liu ZH, Chen J. Investigation of uniaxial low-cycle fatigue failure behavior of hot-rolled AZ91 magnesium alloy. Int J Fatigue 2013;48:122–32. https://doi.org/10.1016/j.ijfatigue.2012.10.010.
[64] Lin YC, Liu ZH, Chen XM, Chen J. Stress-based fatigue life prediction models for AZ31B magnesium alloy under single-step and multi-step asymmetric stress-controlled cyclic loadings. Comput Mater Sci 2013;73:128–38. https://doi.org/10.1016/j.commatsci.2013.02.023.
[65] Delavar H, Mostahsan AJ, Ibrahim H. Corrosion and corrosion-fatigue behavior of magnesium metal matrix composites for bio-implant applications: A review. J Magnesium Alloys 2023;11:1125–61. https://doi.org/10.1016/j.jma.2023.04.010.
[66] Peron M, Bertolini R, Ghiotti A, Torgersen J, Bruschi S, Berto F. Enhancement of stress corrosion cracking of AZ31 magnesium alloy in simulated body fluid thanks to cryogenic machining. J Mech Behav Biomed Mater 2020;101. https://doi.org/10.1016/j.jmbbm.2019.103429.
[67] Wang Z, Wu S, Kang G, Li H, Wu Z, Fu Y, et al. In-situ synchrotron X-ray tomography investigation of damage mechanism of an extruded magnesium alloy in uniaxial low-cycle fatigue with ratchetting. Acta Mater 2021;211. https://doi.org/10.1016/j.actamat.2021.116881.
[68] Li Y, Jahr H, Zhang XY, Leeflang MA, Li W, Pouran B, et al. Biodegradation-affected fatigue behavior of additively manufactured porous magnesium. Addit Manuf 2019;28:299–311. https://doi.org/10.1016/j.addma.2019.05.013.
[69] Guo T, Chen Y, Cao R, Pang X, He J, Qiao L. Cleavage cracking of ductile-metal substrates induced by brittle coating fracture. Acta Mater 2018;152:77–85. https://doi.org/10.1016/j.actamat.2018.04.017.
[70] Zou Y, Wang Y, Wei D, Du Q, Ouyang J, Jia D, et al. In-situ SEM analysis of brittle plasma electrolytic oxidation coating bonded to plastic aluminum substrate: Microstructure and fracture behaviors. Mater Charact 2019;156. https://doi.org/10.1016/j.matchar.2019.109851.
[71] Kappes M, Iannuzzi M, Carranza RM. Pre-Exposure embrittlement and stress corrosion cracking of magnesium alloy AZ31B in chloride solutions. Corrosion 2014;70:667–77. https://doi.org/10.5006/1172.
[72] Jafari S, Raman RKS, Davies CHJ. Stress corrosion cracking of an extruded magnesium alloy (ZK21) in a simulated body fluid. Eng Fract Mech 2018;201:47–55. https://doi.org/10.1016/j.engfracmech.2018.09.002.
[73] Zhou LF, Liu ZY, Wu W, Li XG, Du CW, Jiang B. Stress corrosion cracking behavior of ZK60 magnesium alloy under different conditions. Int J Hydrogen Energy 2017;42:26162–74. https://doi.org/10.1016/j.ijhydene.2017.08.161.
[74] Galvin E, Cummins C, Yoshihara S, Mac Donald BJ, Lally C. Plastic strains during stent deployment have a critical influence on the rate of corrosion in absorbable magnesium stents. Med Biol Eng Comput 2017;55:1261–75. https://doi.org/10.1007/s11517-016-1584-8.
[75] Chen K, Lu Y, Tang H, Gao Y, Zhao F, Gu X, et al. Effect of strain on degradation behaviors of WE43, Fe and Zn wires. Acta Biomater 2020;113:627–45. https://doi.org/10.1016/j.actbio.2020.06.028.
[76] Panindre AM, Raja VS, Ajay Krishnan M. Explanation for anomalous environmentally assisted cracking behaviour of a wrought Mg–Mn alloy in chloride medium. Corros Sci 2017;115:8–17. https://doi.org/10.1016/j.corsci.2016.11.001.
[77] Shi Z, Hofstetter J, Cao F, Uggowitzer PJ, Dargusch MS, Atrens A. Corrosion and stress corrosion cracking of ultra-high-purity Mg5Zn. Corros Sci 2015;93:330–5. https://doi.org/10.1016/j.corsci.2015.01.032.
[78] Raja VS, Padekar BS. Role of chlorides on pitting and hydrogen embrittlement of Mg-Mn wrought alloy. Corros Sci 2013;75:176–83. https://doi.org/10.1016/j.corsci.2013.05.030.
[79] Talesh SAA, Azadi M. High-cycle fatigue testing on AM60 magnesium alloy samples for as-received and pre-corroded conditions in simulated body fluid. J Mater Res Technol 2023;27:1922–34. https://doi.org/10.1016/j.jmrt.2023.10.078.